Received: 15 August 2020 | Revised: 14 January 2021 | Accepted: 22 January 2021

DOI: 10.1002/zamm.202000221

ORIGINAL PAPER

Multiple scattering of flexural waves on Mindlin plates with circular scatterers

Yohei Kinoshita[1] | **Shiro Biwa**[1] | **Zuowei Wang**[2]

[1] Department of Aeronautics and Astronautics, Graduate School of Engineering, Kyoto University, Katsura, Nishikyo-ku, Kyoto 615-8540, Japan

[2] School of Mechano-Electronic Engineering, Xidian University, P. O. Box 188, Xi'an 710071, China

Correspondence
Shiro Biwa, Department of Aeronautics and Astronautics, Graduate School of Engineering, Kyoto University, Katsura, Nishikyo-ku, Kyoto 615-8540, Japan.
Email: biwa@kuaero.kyoto-u.ac.jp

The multiple scattering of flexural waves on an elastic plate with circular scatterers is analyzed in the frequency domain based on the Mindlin plate theory accounting for the rotary inertia and shear deformation of the plate. To this purpose, a semi-analytical numerical method is formulated as an extension of the previous study based on the Kirchhoff plate theory. It consists of expressing the flexural wave field in terms of the superposition of the wave function expansion, and determining the expansion coefficients by a collocation technique. As demonstrative examples, the transmission of a plane flexural wave across a square array of circular through-thickness holes or thin-plate inclusions is analyzed using the proposed method. The comparison between the results based on the Mindlin and Kirchhoff theories is shown for the case of multiple holes. The analysis shows that the transmission amplitude of the flexural wave is reduced at certain frequencies due to the Bragg reflection by the inclusions. In the case of thin-plate inclusions, the resonance of the inclusions also brings about a sharp decrease of the transmission amplitude.

KEYWORDS
flexural waves, mindlin plate theory, multiple scattering, wave function expansion

1 | INTRODUCTION

Scattering of flexural waves by holes, inclusions or other inhomogeneous features in elastic plates has been a subject actively investigated in applied mechanics for its importance in the design of thin-walled structures against dynamic loading. Among the earliest contributions, Pao and Chao [1] analyzed the scattering of a plane flexural wave by a circular hole in an elastic plate and the associated dynamic concentration of bending moment and shear force around it. Later, Paskaramoorthy et al. [2] analyzed the flexural wave scattering by an arbitrarily shaped cavity using a hybrid technique of the analytical wave function expansion and the finite element method. Vemula and Norris [3] presented the formulation of flexural wave scattering for a general class of inhomogeneity and some related aspects of energy flux conservation. More recently, this subject also gained much attention in the context of nondestructive testing and structural health monitoring of plate-like structures using flexural waves. With such applications in the background, Wang and Chang [4] studied the scattering of flexural waves by different types of cylindrical defects and presented some explicit results based on the Born approximation together with experimental results. Cegla et al. [5] studied the flexural wave scattering and the accompanying mode conversion behavior at a circular blind hole on a plate.

For the analysis of flexural motions in isotropic elastic plates, two classical approximate theories are well established, i.e., the Kirchhoff-Love theory [6] (referred to as the Kirchhoff theory below) and the Reissner-Mindlin theory [7] (referred

to as the Mindlin theory), in addition to the rigorous Rayleigh-Lamb theory for the so-called Lamb waves [8, 9]. In the Kirchhoff plate theory, the governing equation is solely described in terms of the out-of-plane deflection of the mid-plane of the plate. Its validity is, however, limited to very thin plates or a rather low frequency range. On the other hand, the Mindlin plate theory takes into account the rotary inertia and shear deformation of the plate and is capable of giving more reasonable prediction of the flexural wave propagation for thicker plates or for a wider range of frequency. The above-mentioned studies of flexural wave scattering [1–5] were based on the Mindlin theory. Corresponding problems of flexural wave scattering based on the Kirchhoff theory have been studied by Norris and Vemula [10], Squire and Dixon [11], Grahn [12], and Fromme and Sayir [13], among others.

In the works mentioned above [1-5, 10-13], the flexural wave scattering was analyzed for a single scatterer in a plate. The level of analytical complexity rises substantially when one aims to study the flexural wave scattering by multiple scatterers. Different investigators [14–18] analyzed the multiple scattering of flexural waves and presented some numerical results for the cases of two or three circular inclusions. Peng [19] applied the acoustic wave propagator method to the problem of flexural wave scattering by nine patches on a plate. In many circumstances, however, there is a need to analyze flexural wave scattering for a greater number of scatterers. In particular, the possibility of manipulating flexural waves in plates by periodic arrangements of inclusions, e.g., filtering, focusing, cloaking, etc., is actively pursued in the current trend of research, i.e., thin-plate versions of phononic crystals and acoustic metamaterials [20–22]. For infinitely extended periodic arrangements of scatterers, the band structure of flexural waves was analyzed by Movchan et al. [23] and Smith et al. [24]. Flexural wave propagation in strongly heterogeneous periodic plates was analyzed by Rohan and Miara [25] based on the two-scale homogenization technique. The flexural wave scattering by a random distribution of inclusions in plates was analyzed by Weaver [26], Dixon and Squire [27] and Parnell and Martin [28] using the statistical treatments. Recently, the multiple scattering of flexural waves by a large number of inclusions was analyzed by Cai and Hambric [29] based on the formalism of multiple scattering theory of waves. Wang and Biwa [30] formulated a computational method for multiple scattering of flexural waves by circular holes based on the wave function expansion and a numerical collocation technique. Similar formulation has been applied by Wang et al. [31] to analyze the multiple scattering of flexural waves by annular inclusions.

As mentioned above, the scattering of flexural waves by inclusions of different types is an important topic in different perspectives ranging over the dynamic stress concentration, nondestructive testing/structural health monitoring, and phononic crystals/acoustic metamaterials. With a few exceptions [15, 25], however, most of the above-mentioned works for the multiple scattering of flexural waves are based on the classical Kirchhoff theory. It is then of definite interest to analyze the multiple scattering of flexural waves based on the Mindlin theory due to its validity for a wider range of plate thickness and frequency. This issue is also worthy of investigation since the more straightforward numerical analysis of the corresponding problem within the framework of three-dimensional elasticity, with the help of commercial software, is still heavily time- and memory-consuming. Therefore, the aim of the present study is to extend the previous work by Wang and Biwa [30] and to establish a numerical method to analyze the multiple scattering of flexural waves based on the Mindlin theory. Namely, the flexural wave fields in an elastic plate with multiple scatterers are expressed as the superposition of the wave function expansion, and their expansion coefficients are obtained numerically by a collocation technique. With the proposed method, some numerical results are demonstrated for the scattering of a plane flexural wave by multiple holes and multiple thin-plate inclusions.

This paper is structured as follows. In Section 2, the basic equations of the Mindlin theory are outlined, and the multiple scattering analysis is formulated on this basis. In Section 3, the setting of some numerical examples, i.e., a square array of through-thickness holes or thin-plate inclusions, is described. In Section 4, the numerical results are demonstrated and discussed, in particular in the light of the stop band formation for the flexural wave. Section 5 summarizes the conclusion of this study.

2 | FORMULATION

2.1 | Mindlin plate theory

The fundamental equations of the Mindlin plate theory [1, 3, 5, 7] are first recapitulated as the basis of the present analysis. For a flat plate of thickness h made of an isotropic linear elastic solid (density ρ, Young's modulus E, Poisson's ratio ν), the

governing equations for the free flexural motion are, in the frequency domain with the angular frequency ω, given by

$$\kappa G h \left(\nabla^2 W + \frac{\partial \Pi_x}{\partial x} + \frac{\partial \Pi_y}{\partial y} \right) + \rho h \omega^2 W = 0, \tag{1}$$

$$\kappa G h \left(\Pi_x + \frac{\partial W}{\partial x} \right) - \frac{D}{2} \left\{ (1-\nu)\nabla^2 \Pi_x + (1+\nu) \frac{\partial}{\partial x} \left(\frac{\partial \Pi_x}{\partial x} + \frac{\partial \Pi_y}{\partial y} \right) \right\} - \frac{\rho h^3}{12} \omega^2 \Pi_x = 0, \tag{2}$$

$$\kappa G h \left(\Pi_y + \frac{\partial W}{\partial y} \right) - \frac{D}{2} \left\{ (1-\nu)\nabla^2 \Pi_y + (1+\nu) \frac{\partial}{\partial y} \left(\frac{\partial \Pi_x}{\partial x} + \frac{\partial \Pi_y}{\partial y} \right) \right\} - \frac{\rho h^3}{12} \omega^2 \Pi_y = 0, \tag{3}$$

where the x-y coordinate system is taken in the mid-plane of the plate. In the above expressions, $W(x, y)$ denotes the mid-plane deflection, $\Pi_x(x, y)$ and $\Pi_y(x, y)$ denote the rotation angles with respect to the y and x axes, respectively, and ∇^2 denotes the two-dimensional Laplacian operator. The parameter κ is the shear correction factor. The shear modulus G and the flexural rigidity D are defined by

$$G = \frac{E}{2(1+\nu)}, \quad D = \frac{E h^3}{12(1-\nu^2)}. \tag{4}$$

The solution to the above governing equations can be expressed as [1, 3]

$$W = W_1 + W_2, \tag{5}$$

$$\Pi_x = \alpha_1 \frac{\partial W_1}{\partial x} + \alpha_2 \frac{\partial W_2}{\partial x} + \frac{\partial V}{\partial y}, \tag{6}$$

$$\Pi_y = \alpha_1 \frac{\partial W_1}{\partial y} + \alpha_2 \frac{\partial W_2}{\partial y} - \frac{\partial V}{\partial x}, \tag{7}$$

where the functions $W_1(x, y)$, $W_2(x, y)$ and $V(x, y)$ satisfy the Helmholtz equations

$$\nabla^2 W_1 + {k_1}^2 W_1 = 0, \quad \nabla^2 W_2 + {k_2}^2 W_2 = 0, \quad \nabla^2 V + {k_3}^2 V = 0, \tag{8}$$

with the wave numbers k_1, k_2 and k_3 given by

$${k_1}^2 = \frac{\rho\omega^2}{2G} \left(\frac{1-\nu}{2} + \frac{1}{\kappa} \right) + \sqrt{\frac{\rho^2\omega^4}{4G^2} \left(\frac{1-\nu}{2} - \frac{1}{\kappa} \right)^2 + \frac{6(1-\nu)\rho\omega^2}{Gh^2}}, \tag{9}$$

$${k_2}^2 = \frac{\rho\omega^2}{2G} \left(\frac{1-\nu}{2} + \frac{1}{\kappa} \right) - \sqrt{\frac{\rho^2\omega^4}{4G^2} \left(\frac{1-\nu}{2} - \frac{1}{\kappa} \right)^2 + \frac{6(1-\nu)\rho\omega^2}{Gh^2}}, \tag{10}$$

$${k_3}^2 = \frac{\rho\omega^2}{G} - \frac{12\kappa}{h^2}. \tag{11}$$

The coefficients α_1 and α_2 in Equations (6) and (7) are given by

$$\alpha_1 = -1 + \frac{{k_s}^2}{{k_1}^2}, \quad \alpha_2 = -1 + \frac{{k_s}^2}{{k_2}^2}, \quad k_s = \frac{\omega}{\sqrt{\kappa} c_{\mathrm{T}}}, \tag{12}$$

where $c_{\mathrm{T}} = \sqrt{G/\rho}$ is the shear wave velocity in the solid. The present analysis focuses on a low-frequency range where $\omega < \sqrt{12\kappa}\, c_{\mathrm{T}}/h$, then k_1^2 is positive while k_2^2 and k_3^2 are negative. In this situation, the wave field given by W_1 represents a propagating flexural wave with a real wave number, and the wave fields given by W_2 and V represent non-propagating (spatially decaying) waves with pure imaginary wave numbers.

For later use, the bending moments M_x, M_y, torque M_{xy} and shear forces Q_x, Q_y in the plate are described here in terms of the deflection W and rotations Π_x, Π_y,

$$M_x = D\left(\frac{\partial \Pi_x}{\partial x} + \nu\frac{\partial \Pi_y}{\partial y}\right), \quad M_y = D\left(\frac{\partial \Pi_y}{\partial y} + \nu\frac{\partial \Pi_x}{\partial x}\right), \quad M_{xy} = \frac{(1-\nu)D}{2}\left(\frac{\partial \Pi_x}{\partial y} + \frac{\partial \Pi_y}{\partial x}\right), \tag{13a}$$

$$Q_x = \kappa G h\left(\Pi_x + \frac{\partial W}{\partial x}\right), \quad Q_y = \kappa G h\left(\Pi_y + \frac{\partial W}{\partial y}\right). \tag{13b}$$

In polar coordinates, the corresponding quantities are given by

$$\Pi_r = \alpha_1\frac{\partial W_1}{\partial r} + \alpha_2\frac{\partial W_2}{\partial r} + \frac{1}{r}\frac{\partial V}{\partial \theta}, \ \Pi_\theta = \alpha_1\frac{1}{r}\frac{\partial W_1}{\partial \theta} + \alpha_2\frac{1}{r}\frac{\partial W_2}{\partial \theta} - \frac{\partial V}{\partial r}, \tag{14a}$$

$$\begin{aligned} M_r &= D\left\{\frac{\partial \Pi_r}{\partial r} + \frac{\nu}{r}\left(\Pi_r + \frac{\partial \Pi_\theta}{\partial \theta}\right)\right\}, \quad M_\theta = D\left\{\frac{1}{r}\left(\Pi_r + \frac{\partial \Pi_\theta}{\partial \theta}\right) + \nu\frac{\partial \Pi_r}{\partial r}\right\}, \\ M_{r\theta} &= \frac{(1-\nu)D}{2}\left\{\frac{1}{r}\left(\frac{\partial \Pi_r}{\partial \theta} - \Pi_\theta\right) + \frac{\partial \Pi_\theta}{\partial r}\right\}, \end{aligned} \tag{14b}$$

$$Q_r = \kappa G h\left(\Pi_r + \frac{\partial W}{\partial r}\right), \quad Q_\theta = \kappa G h\left(\Pi_\theta + \frac{1}{r}\frac{\partial W}{\partial \theta}\right). \tag{14c}$$

2.2 | Multiple scattering of flexural waves

Based on the fundamental relations described above, the scattering of a flexural wave by non-overlapping scatterers distributed on the plate is considered, following the formulation in Ref. [30] based on the Kirchhoff theory and other foregoing works on multiple scattering in fiber-reinforced media [32–34]. The number of the scatterers is denoted by N. It is assumed that all scatterers have the same circular shape of radius R. Two cases are considered in the present analysis, where (i) all scatterers are through-thickness holes, and (ii) all scatterers are circular plate-shaped elastic inclusions of the same thickness $\bar{h}$, density $\bar{\rho}$, Young's modulus $\bar{E}$ and Poisson's ratio $\bar{\nu}$. It is also assumed that the host plate and the inclusions have the common mid-plane and the whole structure is symmetric with respect to it. In this situation, only the flexural motions are generated as an outcome of the interaction of the incident flexural wave with the scatterers: the coupling with the in-plane motions does not occur. The flexural motions of both the host plate and the inclusions are described by the Mindlin plate theory in this paper.

When the incident flexural wave interacts with N scatterers, a multiply scattered wave field is realized on the plate. The resulting wave field can be given in terms of the three wave functions W_1, W_2 and V defined in Equations (5)-(7). As shown in Figure 1, the location of a generic point in the x-y plane is expressed by the position vector $\mathbf{r}$, and the deflection field $W(x, y)$ is also denoted by $W(\mathbf{r})$. The three wave functions associated with the scattered wave by the ith scatterer ($i = 1, 2, \ldots, N$), whose center is located at $\mathbf{r} = \mathbf{r}_i$, satisfy the Helmholtz equations and should meet the radiation condition far away from that scatterer. Therefore, they can be expressed as

$$W_1^{i,\mathrm{sca}}(\mathbf{r}) = \sum_{n=-\infty}^{\infty} A_n^i H_n^{(1)}(k_1|\mathbf{r} - \mathbf{r}_i|)\exp(\mathrm{i}n\theta_i), \tag{15a}$$

$$W_2^{i,\mathrm{sca}}(\mathbf{r}) = \sum_{n=-\infty}^{\infty} B_n^i H_n^{(1)}(k_2|\mathbf{r} - \mathbf{r}_i|)\exp(\mathrm{i}n\theta_i), \tag{15b}$$

$$V^{i,\mathrm{sca}}(\mathbf{r}) = \sum_{n=-\infty}^{\infty} C_n^i H_n^{(1)}(k_3|\mathbf{r} - \mathbf{r}_i|)\exp(\mathrm{i}n\theta_i), \tag{15c}$$

where $H_n^{(1)}(\cdot)$ denotes the nth-order Hankel function of the first kind, A_n^i, B_n^i and C_n^i ($i = 1, 2, \ldots, N$, $n = 0, \pm 1, \pm 2, \ldots$) are unknown expansion coefficients, k_j ($j = 1, 2, 3$) are the wave numbers in the host plate defined in Equations

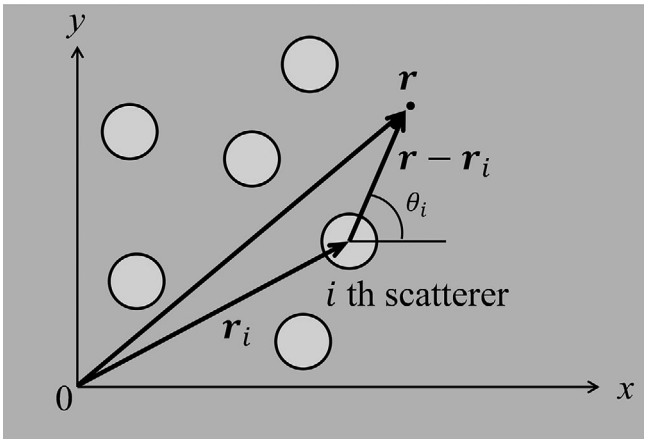

FIGURE 1 An infinitely extended elastic plate with circular scatterers and the coordinate system

(9)-(11), and θ_i denotes the polar angle of a generic point $\mathbf{r}$ viewed from the center of the ith scatterer $\mathbf{r}_i$ as shown in Figure 1.

If the ith scatterer is a through-thickness hole, there is no wave field inside it. If the scatterer is a plate-shaped elastic inclusion, the wave functions inside it should satisfy the Helmholtz equations of Equation (8) and be finite therein, so they can be expressed as

$$W_1^{i,\text{inside}}(\mathbf{r}) = \sum_{n=-\infty}^{\infty} S_n^i J_n(\bar{k}_1|\mathbf{r}-\mathbf{r}_i|)\exp(\mathrm{i}n\theta_i), \tag{16a}$$

$$W_2^{i,\text{inside}}(\mathbf{r}) = \sum_{n=-\infty}^{\infty} T_n^i J_n(\bar{k}_2|\mathbf{r}-\mathbf{r}_i|)\exp(\mathrm{i}n\theta_i), \tag{16b}$$

$$V^{i,\text{inside}}(\mathbf{r}) = \sum_{n=-\infty}^{\infty} U_n^i J_n(\bar{k}_3|\mathbf{r}-\mathbf{r}_i|)\exp(\mathrm{i}n\theta_i), \tag{16c}$$

where $J_n(\cdot)$ denotes the nth-order Bessel function of the first kind, S_n^i, T_n^i and U_n^i $(i = 1, 2, \ldots, N, n = 0, \pm 1, \pm 2, \ldots)$ are unknown expansion coefficients, and $\bar{k}_j$ $(j = 1, 2, 3)$ are the wave numbers in the scatterer defined in Equations (9)-(11) with the parameters of the scatterer.

The scattered wave by the ith scatterer is created in response to the so-called exciting field for that scatterer, which is defined as the wave field in the host plate when that scatterer is not present there. The exciting field is given by the sum of the incident wave and the scattered waves by all the other scatterers, i.e,

$$W_1^{i,\text{exc}}(\mathbf{r}) = W_1^{\text{inc}}(\mathbf{r}) + \sum_{\substack{j=1\\ j\neq i}}^{N} W_1^{j,\text{sca}}(\mathbf{r}), \tag{17a}$$

$$W_2^{i,\text{exc}}(\mathbf{r}) = W_2^{\text{inc}}(\mathbf{r}) + \sum_{\substack{j=1\\ j\neq i}}^{N} W_2^{j,\text{sca}}(\mathbf{r}), \tag{17b}$$

$$V^{i,\text{exc}}(\mathbf{r}) = V^{\text{inc}}(\mathbf{r}) + \sum_{\substack{j=1\\ j\neq i}}^{N} V^{j,\text{sca}}(\mathbf{r}), \tag{17c}$$

where $W_1^{\text{inc}}(\mathbf{r})$, $W_2^{\text{inc}}(\mathbf{r})$ and $V^{\text{inc}}(\mathbf{r})$ are the wave functions of the incident wave which satisfy the Helmholtz equations. Since the waves of the exciting field, $W_1^{i,\text{exc}}(\mathbf{r})$, $W_2^{i,\text{exc}}(\mathbf{r})$ and $V^{i,\text{exc}}(\mathbf{r})$, should satisfy the Helmholtz equations and be finite

at $\mathbf{r} = \mathbf{r}_i$, they can be expressed as

$$W_1^{i,\mathrm{exc}}(\mathbf{r}) = \sum_{n=-\infty}^{\infty} E_n^i J_n(k_1|\mathbf{r}-\mathbf{r}_i|)\exp(\mathrm{i}n\theta_i), \tag{18a}$$

$$W_2^{i,\mathrm{exc}}(\mathbf{r}) = \sum_{n=-\infty}^{\infty} F_n^i J_n(k_2|\mathbf{r}-\mathbf{r}_i|)\exp(\mathrm{i}n\theta_i), \tag{18b}$$

$$V^{i,\mathrm{exc}}(\mathbf{r}) = \sum_{n=-\infty}^{\infty} G_n^i J_n(k_3|\mathbf{r}-\mathbf{r}_i|)\exp(\mathrm{i}n\theta_i), \tag{18c}$$

where E_n^i, F_n^i and G_n^i ($i = 1, 2, \ldots, N$, $n = 0, \pm 1, \pm 2, \ldots$) are unknown expansion coefficients.

The expansion coefficients A_n^i, B_n^i, C_n^i of the scattered wave and S_n^i, T_n^i and U_n^i of the wave inside the scatterer are related to the coefficients E_n^i, F_n^i, G_n^i of the exciting field via the boundary conditions at the interface of each scatterer and the host plate. If the ith scatterer is a through-thickness hole, its boundary is assumed traction-free, so the resulting radial bending moment, torque and radial shear force should vanish, i.e.,

$$M_r^{i,\mathrm{exc}} + M_r^{i,\mathrm{sca}} = 0,\ M_{r\theta}^{i,\mathrm{exc}} + M_{r\theta}^{i,\mathrm{sca}} = 0,\ Q_r^{i,\mathrm{exc}} + Q_r^{i,\mathrm{sca}} = 0, \tag{19}$$

at $|\mathbf{r}-\mathbf{r}_i| = R, 0 \le \theta_i < 2\pi$. In the above expressions, $M_r^{i,\mathrm{exc}}$ denotes the radial bending moment associated with the exciting field for the ith scatterer, and the other quantities are defined similarly.

If the ith scatterer is a plate-shaped inclusion, the elastic constants and the plate thickness can be discontinuous at the boundary: it is then assumed that the radial bending moment, torque and radial shear force as well as the mid-plane deflection and rotation angles are continuous, i.e.,

$$M_r^{i,\mathrm{exc}} + M_r^{i,\mathrm{sca}} = M_r^{i,\mathrm{inside}},\quad M_{r\theta}^{i,\mathrm{exc}} + M_{r\theta}^{i,\mathrm{sca}} = M_{r\theta}^{i,\mathrm{inside}},\quad Q_r^{i,\mathrm{exc}} + Q_r^{i,\mathrm{sca}} = Q_r^{i,\mathrm{inside}}, \tag{20a}$$

$$W^{i,\mathrm{exc}} + W^{i,\mathrm{sca}} = W^{i,\mathrm{inside}},\quad \Pi_r^{i,\mathrm{exc}} + \Pi_r^{i,\mathrm{sca}} = \Pi_r^{i,\mathrm{inside}},\quad \Pi_\theta^{i,\mathrm{exc}} + \Pi_\theta^{i,\mathrm{sca}} = \Pi_\theta^{i,\mathrm{inside}}, \tag{20b}$$

at $|\mathbf{r}-\mathbf{r}_i| = R, 0 \le \theta_i < 2\pi$, where $W^{i,\mathrm{exc}} = W_1^{i,\mathrm{exc}} + W_2^{i,\mathrm{exc}}$ is the deflection of the exciting field, etc. These conditions are a special case of the more general case treated by Cegla et al. [5] where the inclusion and the host plate have misaligned mid-planes. Since the inclusions and the host plate are assumed to have the common mid-plane in the present analysis, no in-plane resulting forces appear in the boundary conditions. The above boundary conditions establish the following relation in the matrix form,

$$[K_n^{\mathrm{hole}}]\begin{pmatrix} A_n^i \\ B_n^i \\ C_n^i \end{pmatrix} = [B_n^{\mathrm{hole}}]\begin{pmatrix} E_n^i \\ F_n^i \\ G_n^i \end{pmatrix}, \tag{21}$$

for the through-thickness hole, and

$$[K_n^{\mathrm{inclusion}}]\begin{pmatrix} A_n^i \\ B_n^i \\ C_n^i \\ S_n^i \\ T_n^i \\ U_n^i \end{pmatrix} = [B_n^{\mathrm{inclusion}}]\begin{pmatrix} E_n^i \\ F_n^i \\ G_n^i \end{pmatrix}, \tag{22}$$

for the plate-shaped inclusion. The 3×3 matrices $[K_n^{\mathrm{hole}}]$ and $[B_n^{\mathrm{hole}}]$ are given by the 3×3 submatrices of the 6×3 matrices $[K_n^{\mathrm{inclusion}}]$ and $[B_n^{\mathrm{inclusion}}]$, respectively. These matrices can be derived in the manner demonstrated in Refs. [3, 5] and their

explicit presentations are omitted here. By multiplying both sides of Equations (21) and (22) by the inverse of the matrix $[K_n^{\text{hole}}]$ or $[K_n^{\text{inclusion}}]$, respectively, the coefficients A_n^i, B_n^i, C_n^i, S_n^i, T_n^i and U_n^i can be expressed in terms of E_n^i, F_n^i, G_n^i in the following way,

$$\begin{pmatrix} A_n^i \\ B_n^i \\ C_n^i \end{pmatrix} = [M_n^{\text{hole}}] \begin{pmatrix} E_n^i \\ F_n^i \\ G_n^i \end{pmatrix}, \tag{23}$$

for the hole and

$$\begin{pmatrix} A_n^i \\ B_n^i \\ C_n^i \\ S_n^i \\ T_n^i \\ U_n^i \end{pmatrix} = [M_n^{\text{inclusion}}] \begin{pmatrix} E_n^i \\ F_n^i \\ G_n^i \end{pmatrix} \tag{24}$$

for the inclusion.

Substituting Equations (15), (18), (23) and (24) into Equation (17), one obtains

$$\sum_{n=-\infty}^{\infty} E_n^i J_n(k_1|\mathbf{r}-\mathbf{r}_i|)\exp(\mathrm{i}n\theta_i) = W_1^{\text{inc}}(\mathbf{r}) + \sum_{\substack{j=1 \\ j\neq i}}^{N} \sum_{m=-\infty}^{\infty} \left(M_{11}^{(m)} E_m^j + M_{12}^{(m)} F_m^j + M_{13}^{(m)} G_m^j \right) H_m^{(1)}(k_1|\mathbf{r}-\mathbf{r}_j|)\exp(\mathrm{i}m\theta_j) \tag{25a}$$

$$\sum_{n=-\infty}^{\infty} F_n^i J_n(k_2|\mathbf{r}-\mathbf{r}_i|)\exp(\mathrm{i}n\theta_i) = W_2^{\text{inc}}(\mathbf{r}) + \sum_{\substack{j=1 \\ j\neq i}}^{N} \sum_{m=-\infty}^{\infty} \left(M_{21}^{(m)} E_m^j + M_{22}^{(m)} F_m^j + M_{23}^{(m)} G_m^j \right) H_m^{(1)}(k_2|\mathbf{r}-\mathbf{r}_j|)\exp(\mathrm{i}m\theta_j) \tag{25b}$$

$$\sum_{n=-\infty}^{\infty} G_n^i J_n(k_3|\mathbf{r}-\mathbf{r}_i|)\exp(\mathrm{i}n\theta_i) = V^{\text{inc}}(\mathbf{r}) + \sum_{\substack{j=1 \\ j\neq i}}^{N} \sum_{m=-\infty}^{\infty} \left(M_{31}^{(m)} E_m^j + M_{32}^{(m)} F_m^j + M_{33}^{(m)} G_m^j \right) H_m^{(1)}(k_3|\mathbf{r}-\mathbf{r}_j|)\exp(\mathrm{i}m\theta_j) \tag{25c}$$

which contain the expansion coefficients of the exciting field E_n^i, F_n^i, G_n^i alone, where $M_{pq}^{(n)}$ is the (p, q) element of $[M_n^{\text{hole}}]$ or $[M_n^{\text{inclusion}}]$ $(p = 1, 2, 3, q = 1, 2, 3)$. It is noted that $M_{pq}^{(n)}$ is common for all scatterers in the present analysis, although it depends on the type of scatterers considered (hole or plate-shaped inclusion).

2.3 | Collocation technique

In order to determine the unknown expansion coefficients E_n^i, F_n^i, G_n^i, the numerical collocation technique, which was used in the previous works [30–34], is also employed here. Namely, the infinite series in Equation (25) are truncated with a finite number of terms, i.e., the infinite sums for $-\infty < n < \infty$ are replaced by those for $-n_{\max} < n < n_{\max}$, where the integer parameter $n_{\max}$ is set large enough to achieve sufficient accuracy. This truncation makes the total number of unknown expansion coefficients to be $3N(2n_{\max}+1)$. In the present numerical analysis, $(2n_{\max}+2)$ collocation points are chosen at equal interval on the boundary of each scatterer, and Equation (25) is evaluated at those points to construct a set of $3N(2n_{\max}+2)$ linear equations for $3N(2n_{\max}+1)$ coefficients E_n^i, F_n^i, G_n^i $(i = 1, 2, \ldots, N, n = 0, \pm1, \pm2, \ldots, \pm n_{\max})$. This over-determined system of equations can be solved by the least-square method based on the generalized inverse matrix. Making the system of equations over-determined in this way has been found to work well in the previous works [30–34] to avoid ill-conditioning of the equations. In passing, however, it should be mentioned here that when the wave function

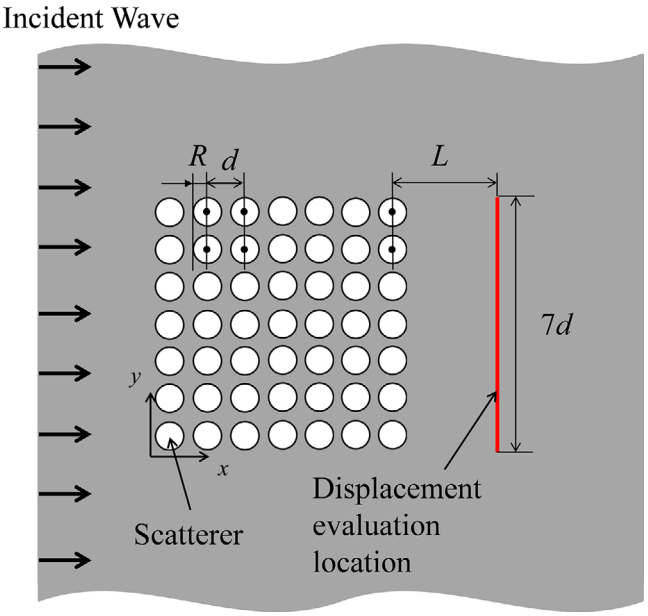

FIGURE 2 Example problem of the flexural wave transmission across a square array of circular scatterers

expansions are applied to multiple scattering problems, a more standard approach is to express the expansions of the scattered fields by the other ($j \neq i$) scatterers in Equation (17) in the single local coordinates around the ith scatterer using Graf's addition theorem [35]. Applying the boundary conditions of Equation (19) or Equation (20), a set of linear equations for the expansion coefficients is obtained without a need to resort to the collocation points. Analytical formulation and numerical implementation of this approach can be found in many references, e.g. [23, 24, 28, 29] for the flexural wave scattering based on the Kirchhoff theory.

Once the coefficients E_n^i, F_n^i, G_n^i are determined, the other expansion coefficients A_n^i, B_n^i, C_n^i, S_n^i, T_n^i and U_n^i can be obtained by Equation (23) or (24). The deflection field on the host plate can be given by

$$\begin{aligned} W(\mathbf{r}) &= W_1(\mathbf{r}) + W_2(\mathbf{r}) \\ &= W_1^{\text{inc}}(\mathbf{r}) + \sum_{j=1}^{N} \sum_{m=-n_{\max}}^{n_{\max}} \left(M_{11}^{(m)} E_m^j + M_{12}^{(m)} F_m^j + M_{13}^{(m)} G_m^j \right) H_m^{(1)}(k_1 |\mathbf{r} - \mathbf{r}_j|) \exp(\mathrm{i}m\theta_j) \\ &\quad + W_2^{\text{inc}}(\mathbf{r}) + \sum_{j=1}^{N} \sum_{m=-n_{\max}}^{n_{\max}} \left(M_{21}^{(m)} E_m^j + M_{22}^{(m)} F_m^j + M_{23}^{(m)} G_m^j \right) H_m^{(1)}(k_2 |\mathbf{r} - \mathbf{r}_j|) \exp(\mathrm{i}m\theta_j) \end{aligned} \tag{26}$$

3 | NUMERICAL EXAMPLES

Based on the formulation given above, the transmission of a plane flexural wave across a square array of circular scatterers is analyzed as demonstrative examples. For the analysis, two types of scatterers are assumed, i.e., (i) through-thickness holes, and (ii) thin-plate inclusions made of the same material as the host plate ($\bar{h} < h, \bar{\rho} = \rho, \bar{E} = E, \bar{\nu} = \nu$). As mentioned above, all scatterers have the same radius R. It is assumed that these scatterers are spatially arranged in a square array with their center-to-center distance d ($> 2R$) as shown in Figure 2. The origin of the x-y coordinate system is chosen so that the center of the bottom left scatterer in the array is located at $(x, y) = (d/2, d/2)$. In the present analysis, the 7×3, 7×5 and 7×7 arrays are considered.

The incident wave is assumed to be a propagating flexural wave of the form

$$W^{\text{inc}}(\mathbf{r}) = W_0 \exp(\mathrm{i}k_1 x), \tag{27}$$

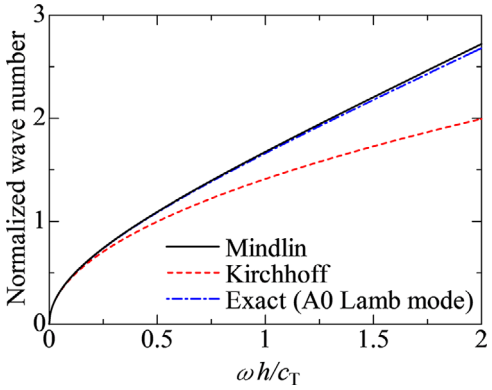

FIGURE 3 Dispersion relations of the flexural wave based on the Mindlin theory, Kirchhoff theory, and the exact theory for the zeroth-order antisymmetric (A0) Lamb wave

where the amplitude W_0 is arbitrarily set as unity owing to the linear nature of the problem. In this case, the three wave functions associated with the incident wave are

$$W_1^{\text{inc}}(\mathbf{r}) = W_0 \exp(\mathrm{i}k_1 x), \quad W_2^{\text{inc}}(\mathbf{r}) = 0, \quad V^{\text{inc}}(\mathbf{r}) = 0. \tag{28}$$

When the incident wave is given, the multiple scattering analysis formulated in the foregoing section yields the wave field in the plate by Equation (26). In the numerical results shown in the following section, the absolute value of the deflection is averaged for a finite length $0 < y < 7d$ at the distance of L from the center of the rightmost scatterers in the array,

$$|W|_{\text{ave}} = \frac{1}{7d} \int_0^{7d} |W(x_{\text{eval}}, y)|\, dy, \tag{29}$$

where $x_{\text{eval}} = 13d/2 + L$, and used as a measure of the magnitude of flexural wave transmitted across the square array of scatterers, partly following the examples demonstrated by Cai and Hambric [29].

In terms of non-dimensional parameters, the transmission behavior of the flexural wave is governed by the non-dimensional frequency $\omega d/c_T$ (or the non-dimensional wave number of the incident wave $k_1 d$), Poisson's ratio ν, the shear correction factor κ, the thickness-scatterer interval ratio h/d, the scatterer radius-interval ratio R/d, and the displacement evaluation distance-scatterer interval ratio L/d. When the scatterers are thin-plate inclusions of the same material, their thickness ratio $\bar{h}/h$ is another governing parameter. In the present analysis, the flexural wave transmission across the square array of scatterers is computed using the fixed values of $\nu = 0.34$, $\kappa = 5/6$ and $L/d = 3$. It is noted that several values have been used for the shear correction factor κ in the literature. While the choice of $\kappa = (c_R/c_T)^2$, where c_R is the Rayleigh surface wave velocity, yields the high-frequency limit of the phase velocity of the propagating wave W_1 which coincides with the Rayleigh wave velocity, the value of $\kappa = \pi^2/12$ gives the cut-off frequencies of the waves W_2 and V which matches to the lowest cut-off frequency of guided wave modes of the plate in the exact theory [36]. Stephen [37] discusses different choices of κ in the light of approximation to the exact theory. In the present analysis, the classical value of $\kappa = 5/6$, due to the static theory of Reissner [38], is used since the frequency range examined here is relatively low and remains below the half of the cut-off frequencies. As a matter of fact, it has been confirmed in the numerical analysis that the two values of $\kappa = 5/6 \cong 0.833$ and $\kappa = \pi^2/12 \cong 0.822$ do not make any noticeable differences in the $|W|_{\text{ave}}$-$\omega d/c_T$ relation in the frequency range $0 < \omega d/c_T < 5$.

The dispersion curve of the propagating flexural wave W_1 of the Mindlin theory is shown in Figure 3 in terms of the normalized wave number $k_1 h$ and the normalized frequency $\omega h/c_T$. The normalized wave number kh of the Kirchhoff theory, given by

$$kh = \{6(1-\nu)\}^{1/4} \sqrt{\frac{\omega h}{c_T}}, \tag{30}$$

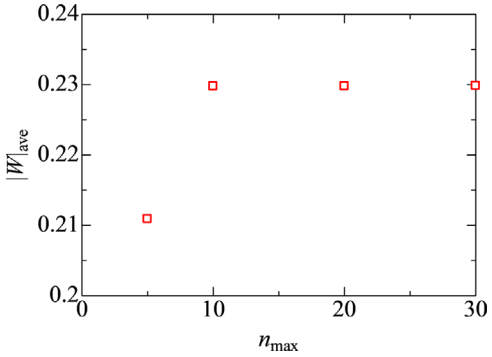

FIGURE 4 Variation of a typical numerical result with the series truncation number

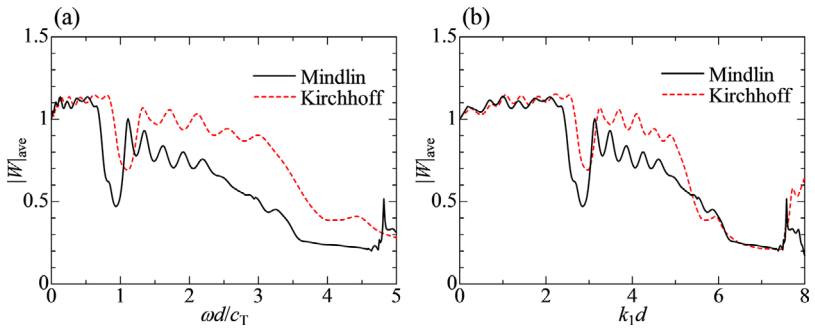

FIGURE 5 Dependence of the transmitted wave amplitude across the 7×7 array of holes ($R/d = 7/16$) on (a) the normalized frequency and (b) the normalized wave number in the host plate, based on the Mindlin and Kirchhoff theories ($h/d = 0.25$)

and the normalized wave number of the lowest-order antisymmetric (A0) mode of Lamb waves are shown for comparison in Figure 3. Since the present analysis is performed for $0 < \omega d/c_T < 5$ and $h/d \leq 0.25$, the relevant range of $\omega h/c_T$ is $0 < \omega h/c_T < 1.25$. It is found in Figure 3 that the Mindlin theory reproduces the exact dispersion relation of the A0 mode Lamb wave with excellent accuracy in the frequency range examined in this paper.

In the numerical analysis, the truncation parameter n_{max} should be set large enough to achieve sufficient convergence of the solution. Generally speaking, a greater n_{max} is necessary for a higher concentration of scatterers (higher R/d) or for a higher frequency. This has been checked for a representative problem of the plate with $h/d = 0.25$ containing the 7×7 square array of holes of radius $R/d = 7/16 = 0.4375$ for the normalized frequency of $\omega d/c_T = 4.25$, corresponding to the largest R/d and a frequency close to the upper limit of the present analysis. The values of $|W|_{ave}$ calculated using different n_{max} are shown in Figure 4. It can be seen in Figure 4 that the value of n_{max} greater than 10 is sufficient to obtain the converged solution. It has also been confirmed that the $|W|_{ave}$-$\omega d/c_T$ curve for this problem, to be shown below, obtained with $n_{max} = 20$ is indistinguishable from that obtained with $n_{max} = 30$. Therefore, the numerical results obtained with $n_{max} = 20$ will be shown in the following section.

4 | RESULTS AND DISCUSSION

4.1 | Through-thickness holes

For the plate of $h/d = 0.25$ with the 7×7 square array of holes with $R/d = 7/16$, the transmitted wave amplitude $|W|_{ave}$ is plotted against the normalized frequency $\omega d/c_T$ in Figure 5a, and against the normalized wave number $k_1 d$ in the host plate in Figure 5b. In Figure 5a, the transmitted wave amplitude shows a dip at around $\omega d/c_T = 1$, and another wider one at around $\omega d/c_T = 4$. These dips are associated with the stop bands of the periodic square array of holes, where the back-scattered waves from different scatterers interfere constructively and prohibit the wave transmission. Rigorously speaking, the term of stop band is defined for infinitely extended periodic structures. In this paper, this term is also used to refer to the frequency (or frequency range) for which the transmission is reduced due to the same mechanism. The stop bands occur when the so-called Bragg condition is satisfied, i.e., $k^{eff} d = m\pi$ (m: integer) [30], where k^{eff} is the effective wave number in the perforated plate. At relatively low frequencies, this wave number does not deviate significantly from the

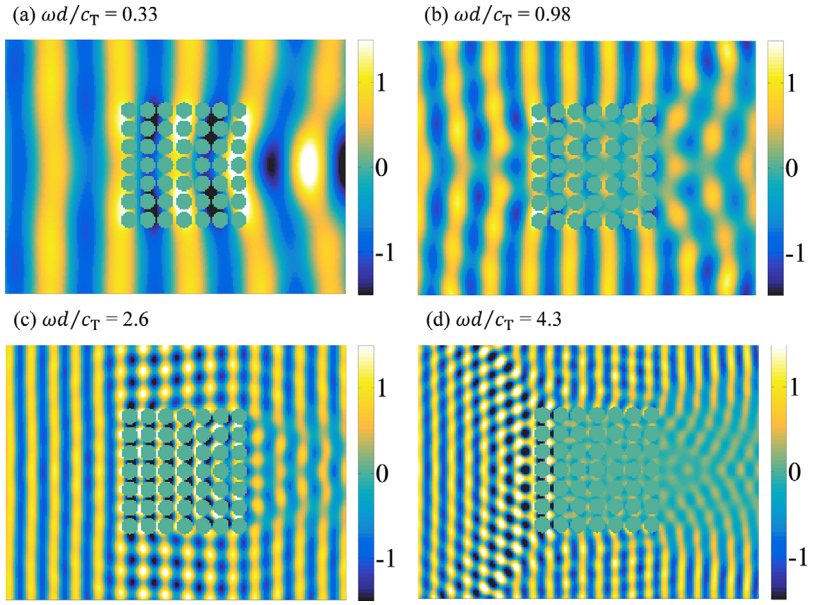

FIGURE 6 Deflection distributions at different normalized frequencies, (a) $\omega d/c_T = 0.33$, (b) $\omega d/c_T = 0.98$, (c) $\omega d/c_T = 2.6$ and (d) $\omega d/c_T = 4.3$

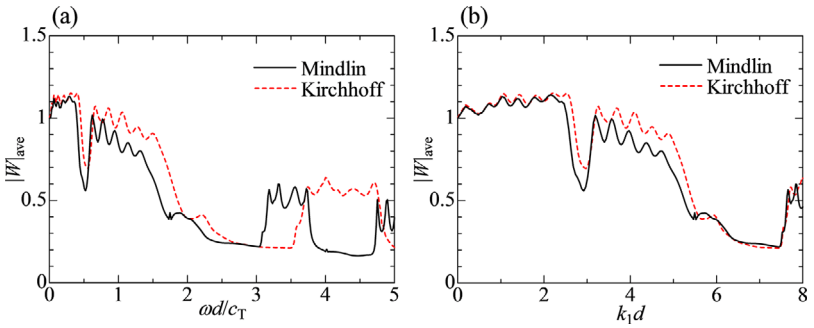

FIGURE 7 Dependence of the transmitted wave amplitude across the 7×7 array of holes ($R/d = 7/16$) on (a) the normalized frequency and (b) the normalized wave number in the host plate, based on the Mindlin and Kirchhoff theories ($h/d = 0.125$)

corresponding wave number of the host plate. As a consequence, the stop bands are expected to appear when $k_1 d \approx m\pi$. An approximate fulfillment of this condition can be confirmed in Figure 5b, where the dips are located near $k_1 d = \pi$ and $k_1 d = 2\pi$. In Figure 5b, the first dip appears to be located slightly lower than $k_1 d = \pi$. This can be explained by the effect of holes which lowers the flexural wave velocity and makes the effective wave number greater than the wave number of the host plate for a given frequency.

The deflection fields around the array of holes, i.e., the spatial distribution of Re[W], are shown in Figure 6 for different normalized frequencies. At a low frequency ($\omega d/c_T = 0.33$), the flexural wave is almost fully transmitted across the array. Since the presence of holes lowers the wave velocity, the flexural wave is diffracted around the square array and tends to be focused ahead of it giving higher local amplitudes. In the first stop band ($\omega d/c_T = 0.98$), the wave length in the array region matches twice the hole interval. Although the Bragg condition is met for this frequency, the flexural wave is partially transmitted across the array, corresponding to the value of $|W|_{ave}$ which is around 0.5 in Figure 5a. At the frequency $\omega d/c_T = 2.6$, the wave is transmitted across the array to a certain amount ($|W|_{ave} = 0.6$ roughly), as also shown in Figure 6c. Finally, in the wider stop band ($\omega d/c_T = 4.3$), the wave transmission is suppressed significantly. At this frequency, the wave has decayed in the array region within the distance of a few columns of holes.

In Figure 5, the numerical results based on the Mindlin and the Kirchhoff theories are compared (in Figure 5b, the normalized wave number kd, given by Equation (30) with $h/d = 0.25$, is taken in the horizontal axis for the Kirchhoff theory). In Figure 5a, the two theories give different results regarding both the overall curves and the location of the stop bands. This is due to the difference of the dispersion relations of the two theories as shown in Figure 3. Furthermore, the wave numbers of the non-propagating modes are also different for the two theories. On the other hand, when plotted against the normalized wave number as in Figure 5b, the transmission behavior at lower frequencies and the location of the stop bands for the two theories are somewhat closer. To examine the correspondence between the two theories further, the numerical results are shown in Figure 7 by reducing the plate thickness to half, i.e., $h/d = 0.125$. In this case, the results are in even closer agreement in Figure 7b, while they show significant difference in Figure 7a. The fair agreement of the

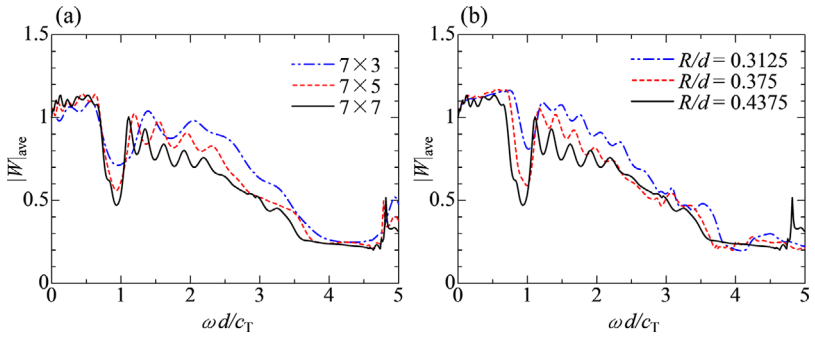

FIGURE 8 Dependence of the transmitted wave amplitude on the normalized frequency ($h/d = 0.25$), (a) for the 7×3, 7×5 and 7×7 arrays of holes with $R/d = 7/16$ and (b) for the 7×7 array of holes with $R/d = 5/16$, 6/16 and 7/16

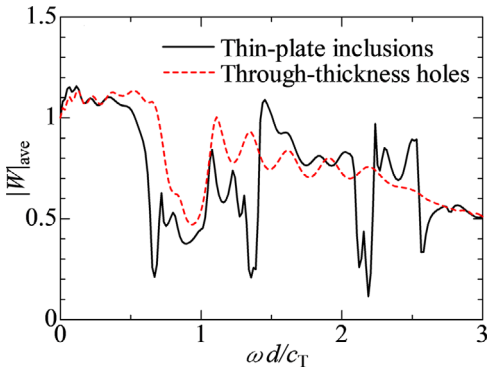

FIGURE 9 Dependence of the transmitted wave amplitude across the 7×7 array of thin-plate inclusions ($R/d = 7/16$) on the normalized frequency ($h/d = 0.25$, $\bar{h}/h = 0.1$)

two theories in terms of the wave number is more or less expected, since the stop band features are governed by the relation $k_1 d$ (or kd) $\approx m\pi$ irrespective of the dispersion relation.

The $|W|_{\text{ave}}$-$\omega d/c_{\text{T}}$ relations for the case of $h/d = 0.25$ are shown for different arrangements (7×3, 7×5 and 7×7) of holes with $R/d = 7/16$ in Figure 8a, and for the 7×7 array of holes with different hole radii $R/d = 5/16 = 0.3125$, $6/16 = 0.375$ and $7/16 = 0.4375$ in Figure 8b. In these results, it is seen that the dip corresponding to the first stop band becomes deeper as the number of hole columns or the hole radius is increased. This is expected because the Bragg reflection is more enhanced with more columns of holes, and larger holes have stronger scattering effects. In contrast, the dip corresponding to the wider stop band is relatively unchanged when these parameters are varied, which indicates that the flexural wave transmission is almost fully suppressed with the smallest number of hole columns or with the smallest radius of holes.

4.2 | Thin-plate inclusions

The transmitted wave amplitude for the plate ($h/d = 0.25$) with the 7×7 array of thin-plate inclusions with $R/d = 7/16$ and $\bar{h}/h = 0.1$ is shown in Figure 9 as a function of the normalized frequency $\omega d/c_{\text{T}}$. The corresponding result for the 7×7 array of through-thickness holes of the same radius is also shown for comparison. In Figure 9, the plate with thin-plate inclusions shows a dip at around $\omega d/c_{\text{T}} = 1$ due to the Bragg reflection as in the case of the plate with through-thickness holes. For the plate with thin-plate inclusions, however, even shaper dips appear at several other frequencies, namely, at $\omega d/c_{\text{T}} = 0.67$, 1.4, and so on. The wave fields around the inclusions (distribution of Re[W]) are shown in Figure 10 for $\omega d/c_{\text{T}} = 0.67$, 0.98 and 1.4 for which the transmitted wave amplitude is relatively low. In Figure 10, the wave fields in the same area as in Figure 6 are shown on the left with the same color scale for -1.5 < Re[W] < 1.5, but the inclusions have much larger deflection out of this range. The wave fields in the full scales are shown on the right for the array region to better reveal the deflection of the inclusions. In Figure 10a for $\omega d/c_{\text{T}} = 0.67$, the inclusions show greater deflections near the left border of the array region, where the inclusions in the neighboring columns are deflected out of phase to each other. In Figure 10b for $\omega d/c_{\text{T}} = 0.98$, the deflection field of the host plate is fairly similar to that in Figure 6b for the plate with through-thickness holes at the same frequency. At this frequency, the deflection amplitudes of the inclusions remain only a few times of that of the host plate. In Figure 10c for $\omega d/c_{\text{T}} = 1.4$, large deflections are seen for inclusions at different

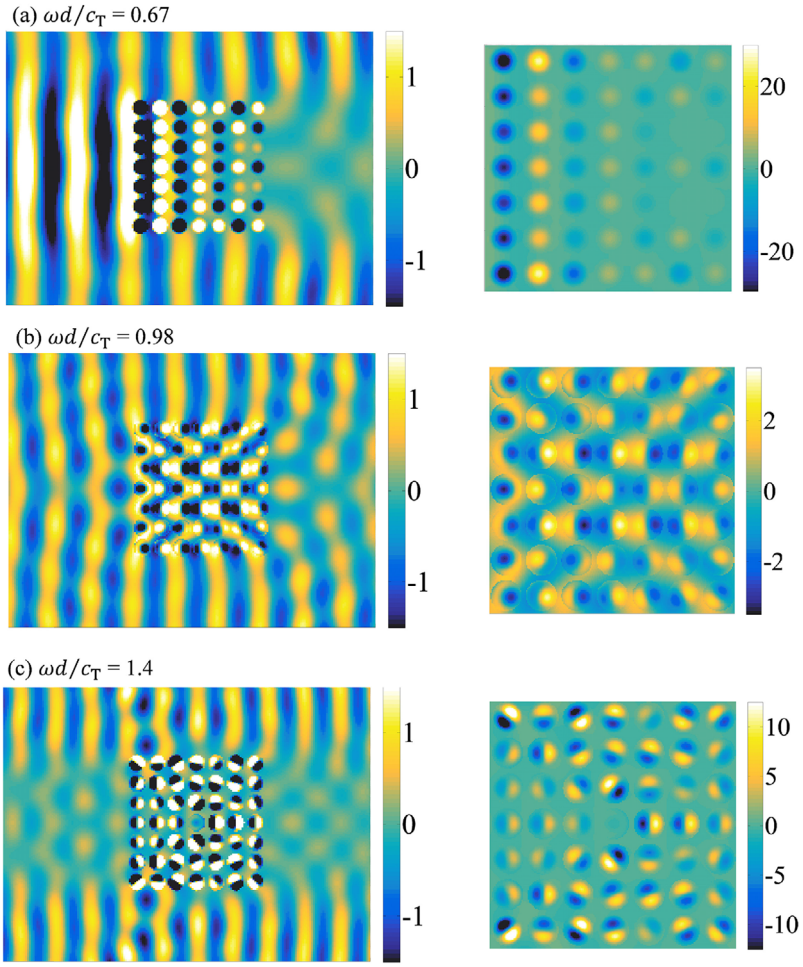

FIGURE 10 Deflection distributions at different normalized frequencies, (a) $\omega d/c_T = 0.67$, (b) $\omega d/c_T = 0.98$ and (c) $\omega d/c_T = 1.4$

locations in the array. Each inclusion is divided into two semi-circles showing opposite deflections, with their orientations being different depending on their location in the array.

Significantly large deflections of the inclusions at the frequencies $\omega d/c_T = 0.67$ and 1.4 indicate that they are at resonance with the incident flexural wave. For the Mindlin theory, the natural frequencies of circular plates are available in the literature only for special material constants and size [39]. Instead, the Kirchhoff theory can be a reasonable approximation for the thin inclusions. Furthermore, the thicker host plate plays a role close to the clamped boundaries to the inclusions. According to the Kirchhoff theory [40], the natural frequencies of a circular plate of thickness $\bar{h}$ and radius R are given by

$$\frac{\omega_{mn}\bar{h}}{c_T} = \frac{\lambda_{mn}}{\sqrt{6(1-\nu)}}\left(\frac{\bar{h}}{R}\right)^2, \tag{31}$$

where m and n are the integer parameters representing the number of node circles and node diameters, respectively. The factors λ_{mn} ($m = 0, 1, 2, \ldots$; $n = 0, 1, 2, \ldots$) are determined by the boundary condition. The factors λ_{mn} for the four lowest natural frequencies of a clamped circular plate are, $\lambda_{mn} = 10.22$ for $(m, n) = (0, 0)$, $\lambda_{mn} = 21.26$ for $(m, n) = (0, 1)$, $\lambda_{mn} = 34.88$ for $(m, n) = (0, 2)$ and $\lambda_{mn} = 39.77$ for $(m, n) = (1, 0)$ [40]. These give $\omega_{00}d/c_T = 0.67$ for $(m, n) = (0, 0)$, $\omega_{01}d/c_T = 1.40$ for $(m, n) = (0, 1)$, $\omega_{02}d/c_T = 2.29$ for $(m, n) = (0, 2)$ and $\omega_{10}d/c_T = 2.61$ for $(m, n) = (1, 0)$, which correspond to the dip frequencies in Figure 9, $\omega d/c_T = 0.67, 1.36, 2.12$ (and 2.19) and 2.56, in reasonable agreement. Furthermore, the deflection distribution in Figure 10a (right) shows the lowest resonant mode for $(m, n) = (0, 0)$, and that in Figure 10c (right) shows the resonant mode for $(m, n) = (0, 1)$ with a single node diameter. This confirms that the dips of the transmitted wave amplitude are due to the resonance of the inclusions. In fact, the introduction of local resonators in the host medium is known as a way to implement an efficient wave suppression mechanism in acoustic metamaterials [22].

As a final remark, it is noted that the flexural wave scattering by the inclusions arranged in a finite square region has been demonstrated in the example presented here. The analysis has shown that the inclusions exhibit oscillation with different magnitudes and orientations depending on their position in the region, as most clearly shown in Figure 10c. This is a feature created by a large but finite number of scatterers arranged in a finite region, which may not be predicted by the more common band-structure analysis based on the Bloch theorem assuming infinitely extended periodic arrangements. The numerical method formulated in the present work is particularly suitable for the analysis of such situations.

5 | CONCLUSION

In this paper, the multiple scattering of flexural waves on an elastic plate with circular scatterers has been analyzed in the frequency domain based on the Mindlin plate theory. To this purpose a semi-analytical numerical method has been formulated as an extension of the previous work based on the Kirchhoff plate theory, which consists of expressing the flexural wave field in terms of the superposition of the wave function expansion and determining the expansion coefficients by a collocation technique. As demonstrative examples, the transmission of a plane flexural wave across a square array of circular scatterers, i.e., through-thickness holes and thin-plate inclusions, have been analyzed. In the case of circular holes, the stop band formation has been observed due to the Bragg reflection. It has been shown that the results based on the Mindlin and Kirchhoff theories are in better agreement for a thinner plate. In the case of circular thin-plate inclusions, a sharp reduction of transmission amplitude has been found due to the flexural resonance of inclusions in addition to the Bragg reflection. Since the Mindlin theory gives a reasonable description of wave motions in elastic plates in a low-frequency range, the present numerical technique can be employed to analyze a wide class of plate-type phononic crystals or acoustic metamaterials. The present analysis has been limited to the situation of inclusions whose geometry is symmetric with respect to the mid-plane of the host plate, so that the flexural waves are not coupled to the extensional or shear horizontal waves. Extension of the analysis to the coupled problems remains as an intriguing issue for further study.

ACKNOWLEDGEMENT

The authors thank Mr. Y. Kishida, a graduate student of Kyoto University, for his assistance in performing supplementary computations.

ORCID

Shiro Biwa https://orcid.org/0000-0001-7278-0462

REFERENCES

[1] Pao, Y. - H., Chao, C. C.: Diffractions of flexural waves by a cavity in an elastic plate. AIAA J. 2, 2004–2010 (1964)
[2] Paskaramoorthy, R., Shah, A.H., Datta, S.K.: Scattering of flexural waves by cavities in a plate. Int. J. Solids Struct. 25, 1177-1191 (1989)
[3] Vemula, C., Norris, A.N.: Flexural wave propagation and scattering on thin plates using Mindlin theory. Wave Motion 26, 1-12 (1997)
[4] Wang, C.H., Chang, F.-K.: Scattering of plate waves by a cylindrical inhomogeneity. J. Sound Vib. 282, 429-451 (2005)
[5] Cegla, F.B., Rohde, A., Veidt, M.: Analytical prediction and experimental measurement for mode conversion and scattering of plate waves at non-symmetric circular blind holes in isotropic plates. Wave Motion 45, 162-177 (2008)
[6] Love, A.E.H.: On the small free vibrations and deformations of elastic shells. Phil. Trans. R. Soc. A17, 491-549 (1888)
[7] Mindlin, R.D.: Influence of rotary inertia and shear on flexural motions of isotropic, elastic plates. ASME J. Appl. Mech. 18, 31-38 (1951)
[8] Rayleigh, J.W.S.: On the free vibrations of an infinite plate of homogeneous isotropic elastic matter. Proc. Lond. Math. Soc. 20, 225-234 (1889)
[9] Lamb, H.: On waves in an elastic plate. Proc. R. Soc. Lond. 93, 114-128 (1917)
[10] Norris, A.N., Vemula, C.: Scattering of flexural waves on thin plates. J. Sound Vib. 118, 115-125 (1995)
[11] Squire, V.A., Dixon, T.W.: Scattering of flexural waves from a coated cylindrical anomaly in a thin plate. J. Sound Vib. 236, 367-373 (2000)
[12] Grahn, T.: Lamb wave scattering from a circular partly through-thickness hole in a plate. Wave Motion 37, 63-80 (2003)
[13] Fromme, P., Sayir, M.F.: Measurement of the scattering of a Lamb wave by a through hole in a plate. J. Acoust. Soc. Am. 111, 1165-1170 (2002)
[14] Saito, H., Nagaya, K.: Flexural wave propagation in a thin plate with circular holes. Bull. JSME 16, 1045-1052 (1973)
[15] Saito, H., Nagaya, K.: Flexural wave propagation in a plate with circular holes. Bull. JSME 16, 1506-1512 (1973)
[16] Chan, K.L., Smith, B., Wester, E.: Flexural wave scattering in a quarter-infinite thin plate with circular scatterers. Int. J. Solids Struct. 46, 3669-3676 (2009)

[17] Lee, W.M., Chen, J.T.: Scattering of flexural wave in a thin plate with multiple circular inclusions by using the null-field integral equation approach. J. Sound Vib. 329, 1042-1061 (2010)
[18] Lee, W.M., Chen, J.T.: Scattering of flexural wave in a thin plate with multiple circular inclusions by using the multipole method. Int. J. Mech. Sci. 53, 617-627 (2011)
[19] Peng, S.Z.: Flexural wave scattering and dynamic stress concentration in a heterogeneous plate with multiple cylindrical patches by acoustical wave propagator technique. J. Sound Vib. 286, 729-743 (2005)
[20] Wu, T.-T., Hsu, J.-C., Sun, J.-H.: Phononic plate waves. IEEE Trans. Ultrason. Ferroelect. Freq. Contr. 58, 2146-2161 (2011)
[21] Mohammadi, S., Adibi, A.: Phononic crystal membranes (slabs or plates), In: Khelif, A., Adibi, A. (eds.) Phononic Crystals, pp. 109-143. Springer, New York (2016)
[22] Huang, T.-Y., Shen, C., Jing, Y.: Membrane- and plate-type acoustic metamaterials. J. Acoust. Soc. Am. 139, 3240-3250 (2016)
[23] Movchan, A.B., Movchan, N.V., McPhedran, R.C.: Bloch-Floquet bending waves in perforated thin plates. Proc. R. Soc. A463, 2505-2518 (2007)
[24] Smith, M.J.A., Meylan, M.H., McPhedran, R.C., Poulton, C.G.: A short remark on the band structure of free-edge platonic crystals. Waves Random Complex 24, 421-430 (2014)
[25] Rohan, E., Miara, B.: Elastodynamics of strongly heterogeneous periodic plates using Reissner-Mindlin and Kirchhoff-Love models. ZAMM Z. Angew. Math. Mech. 96, 304-326 (2016)
[26] Weaver, R.L.: Multiple-scattering theory for mean responses in a plate with sprung masses. J. Acoust. Soc. Am. 101, 3466-3474 (1997)
[27] Dixon, T.W., Squire, V.A.: Energy transport velocity of flexural waves in a random medium. Waves Random Media 10, 83-102 (2000)
[28] Parnell, W.J., Martin, P.A.: Multiple scattering of flexural waves by random configurations of inclusions in thin plates. Wave Motion 48, 161-175 (2011)
[29] Cai, L.-W., Hambric, S.A.: Multiple scattering of flexural waves on thin plates. ASME J. Vib. Acoust. 138, 011009 (2016)
[30] Wang, Z., Biwa, S.: Multiple scattering and stop band characteristics of flexural waves on a thin plate with circular holes. J. Sound Vib. 416, 80-93 (2018)
[31] Wang, Z., Li, T., Dong, H.: Flexural wave scattering by varying-thickness annular inclusions on infinite thin plates. Int. J. Mech. Sci. 159, 406-416 (2019)
[32] Biwa, S., Yamamoto, S., Kobayashi, F., Ohno, N.: Computational multiple scattering analysis for shear wave propagation in unidirectional composites. Int. J. Solids Struct. 41, 435-457 (2004)
[33] Kobayashi, F., Biwa, S., Ohno, N.: Wave transmission characteristics in periodic media of finite length: multilayers and fiber arrays. Int. J. Solids Struct. 41, 7361-7375 (2004)
[34] Sumiya, T., Biwa, S., Haïat, G.: Computational multiple scattering analysis of elastic waves in unidirectional composites. Wave Motion 50, 253-270 (2013)
[35] Martin, P.A.: Multiple Scattering: Interaction of Time-Harmonic Waves with N Obstacles, pp. 36-40. Cambridge Univ. Press, Cambridge (2006)
[36] Graff, K.F.: Wave Motion in Elastic Solids. Dover, New York 492-494 (1975)
[37] Stephen, N.G.: Mindlin plate theory: best shear coefficient and higher spectra validity. J. Sound. Vib. 202, 539-553 (1997)
[38] Reissner, E.: On bending of elastic plates. Q. Appl. Math. 5, 55-68 (1947)
[39] Irie, T., Yamada, G., Aomura, S.: Natural frequencies of Mindlin circular plates. ASME J. Appl. Mech. 47, 652-655 (1980)
[40] Leissa, A.W.: Vibration of Plates, NASA SP-160, National Aeronautics and Space Administration, Washington, D.C. 7-35 (1969)

How to cite this article: Kinoshita Y, Biwa S, Wang Z. Multiple scattering of flexural waves on Mindlin plates with circular scatterers. *Z Angew Math Mech*. 2021; e202000221. https://doi.org/10.1002/zamm.202000221